

Article

Roles of Self-Assembly and Secondary Structures in Antimicrobial Peptide Coatings

Xiao Zhu ¹, Weilong Tang ¹, Xinyi Cheng ², Huihui Wang ², Ting Sang ^{2,*} and Zhou Ye ^{3,*}

¹ The State Key Laboratory Breeding Base of Basic Science of Stomatology (Hubei-MOST) & Key Laboratory of Oral Biomedicine Ministry of Education, School and Hospital of Stomatology, Wuhan University, Wuhan 430072, China

² School of Stomatology of Nanchang University & Jiangxi Province Clinical Research Center for Oral Diseases & The Key Laboratory of Oral Biomedicine, Nanchang 330006, China

³ Applied Oral Sciences and Community Dental Care, Faculty of Dentistry, The University of Hong Kong, Hong Kong, China

* Correspondence: sangting3@ncu.edu.cn (T.S.); zhouye22@hku.hk (Z.Y.)

Abstract: Antimicrobial peptide (AMP) coatings are promising alternatives to conventional antibiotics for the prevention of medical device- and implant-associated infections. Compared to covalent immobilization methods, coatings relying on physical interactions are more versatile but usually less stable. Previous work has developed stable noncovalent coatings on titanium and hydroxyapatite with a model AMP, GL13K, leveraging the strong hydrogen bonding between β -sheet-formed self-assemblies and polar substrates. In this work, a different GL13K self-assembly process was triggered with the formation of α -helices in ethanol/water cosolvent. We compared three different coatings on titanium to investigate the roles of self-assembly and secondary structures, including free GL13K in unordered structures, self-assembled GL13K with the formation of α -helices, and self-assembled GL13K with the formation of β -sheets. X-ray photoelectron spectroscopy, Fourier transform infrared spectroscopy, and water contact angle results confirmed the successful coatings of all three physisorbed GL13K conditions. Self-assembled GL13K, either in α -helices or β -sheets, formed more effective antimicrobial coatings in killing Gram-positive *Staphylococcus aureus* than free GL13K. These findings could help design more stable and effective antimicrobial coatings using self-assembled AMPs.

Keywords: antimicrobial peptide; self-assembly; α -helices; β -sheets; amphiphilicity; antimicrobial coating



Citation: Zhu, X.; Tang, W.; Cheng, X.; Wang, H.; Sang, T.; Ye, Z. Roles of Self-Assembly and Secondary Structures in Antimicrobial Peptide Coatings. *Coatings* **2022**, *12*, 1456. <https://doi.org/10.3390/coatings12101456>

Academic Editors: Irina Negut and Valentina Grumezescu

Received: 27 June 2022

Accepted: 22 September 2022

Published: 2 October 2022

Publisher's Note: MDPI stays neutral with regard to jurisdictional claims in published maps and institutional affiliations.



Copyright: © 2022 by the authors. Licensee MDPI, Basel, Switzerland. This article is an open access article distributed under the terms and conditions of the Creative Commons Attribution (CC BY) license (<https://creativecommons.org/licenses/by/4.0/>).

1. Introduction

Bacterial infection associated with medical devices and implants has been a global emerging problem with elevated healthcare costs and increased rates of morbidity and mortality. Biomaterials' surfaces are susceptible to bacterial adhesion and colonization and the formation of biofilms, which are more difficult to kill compared to planktonic bacteria [1,2]. The increasing prevalence of bacterial resistance has further hampered the treatment by traditional antibiotics [3]. Instead of eradicating biofilms after the occurrence of device- and implant-associated infections, antimicrobial coatings have been explored to prevent the biofilm formation by direct contact killing and/or releasing antimicrobial agents [4].

Antimicrobial peptides (AMPs) are promising alternatives to overcome bacterial resistance with broad-spectrum antimicrobial activity and have been developed as coatings on devices and implants [5,6], including titanium implants [7–9], catheters [10,11], and contact lenses [12,13]. Covalent immobilization of AMPs requires the rational designs of chemical coupling strategies, the spaces between AMPs and substrates, and the peptide orientations and flexibility [14]. In comparison, physical coating strategies, such as layer-by-layer (LbL) [15] or the adsorption onto an intermediate layer (e.g., calcium phosphate [16]

and TiO₂ nanotubes [17]), provide a simpler fabrication process but usually result in low coating densities and stability.

In previous work, we developed stable antimicrobial coatings using a model AMP, GL13K, onto the surfaces of titanium [18], dentin [19], and mineralized collagen scaffolds [20]. As a cationic and amphiphilic peptide, GL13K was found to self-assemble into twisted nanoribbons by partially neutralizing the positive charges in alkaline solutions [21,22]. Using a quartz crystal microbalance with dissipation monitoring (QCM-D), we quantitatively demonstrated a significant increase in the adsorption of self-assembled GL13K on hydroxyapatite sensors compared to free GL13K [23]. Peptide self-assembly is a hierarchical process starting with the formation of secondary structures, such as β -sheets in the GL13K nanoribbons [24]. Thus, it is unclear whether the strong interactions between GL13K and the substrate surfaces were mainly established by the self-assembled nanostructures or the formed β -sheets.

It has been studied that the antimicrobial activity of AMPs is highly dependent on the structures of AMPs, including size, charge, hydrophobicity, amphipathicity, and secondary structures [25]. Recently, we demonstrated that the self-assembly dynamics of GL13K were also closely related to the antimicrobial activity [21,22,26]. Though the exact mechanism of action is still unknown, it is generally thought that AMPs might cause the permeation and rupture of the bacterial cell membrane by interacting with the negatively charged constituent phospholipids and peptidoglycan. The effects of self-assembly and secondary structures on the interactions with the bacterial membrane are also difficult to decouple, as the self-assembly process is usually associated with the change in secondary structures.

In this study, we distinguished the roles of self-assembly and secondary structures by triggering a different self-assembly process with α -helices formation in ethanol/water cosolvent. The antimicrobial activities were compared among GL13K coatings prepared in three different conditions, including free and unordered GL13K, self-assembled GL13K with the formation of α -helices, and self-assembled GL13K with the formation of β -sheets.

2. Materials and Methods

2.1. Preparation of Peptide Samples in Ethanol Solutions

GL13K (GKIIKLKASLKLL-NH₂, MW of 1424 g/mol) were purchased from AAPPTec, LLC (Louisville, KY, USA) or Bankpeptide, Ltd. (Hefei, China) with purity > 98%. A stock solution of 10 mM GL13K was prepared in deionized (DI) water and further diluted to 0.1 mM in DI water or ethanol solutions with final ethanol volume fractions of 10%, 50%, 90%, and 99%.

2.2. Circular Dichroism (CD)

CD spectra of the prepared 0.1 mM GL13K solutions were measured using a Jasco J-815 CD spectrometer (Tokyo, Japan) with a 1 mm pathlength quartz cuvette. Three measurements were obtained over a wavelength of 190–260 nm and averaged for each sample. Data with HT voltage > 900 V were excluded in the plots. All CD spectra were corrected by subtracting the solvent background. Estimations for the secondary structure fractions were performed using the CDPro software (<https://www.bmb.colostate.edu/cdpro/>, accessed on 24 September 2022) with a reference set of 48 proteins. All estimations were analyzed using three methods in the software package (SELCON3, CDSSTR, and CONTIN) and averaged for each sample.

2.3. Transmission Electron Microscopy (TEM)

Nanostructures of GL13K in a 90% ethanol solution and a pH = 10.1 M carbonate–bicarbonate buffer solution were visualized by TEM. TEM samples were prepared by depositing 3 μ L of 0.1 mM GL13K solutions on glow-discharged 400-mesh copper grids with carbon films (Ted Pella, Inc., Redding, CA, USA) and stained with 5 μ L of 0.75% uranyl formate. TEM was operated using a FEI Tecnai G2 F30 instrument (Hillsboro, OR, USA) at an accelerating voltage of 300 kV.

2.4. X-ray Photoelectron Spectroscopy (XPS)

An EscaLab 250Xi X-ray photoelectron spectrometer (Thermo Fisher, Waltham, MA, USA) with a monochromatic Al K α X-ray source (45°, 1486.6 eV, 50 W) was used to determine the elemental composition of each sample under ultra-high vacuum (10⁻⁸ Pa). Survey spectra of four samples in each group were measured at 0–1100 eV using a pass energy of 280 eV with a step size of 1.0 eV.

2.5. Fourier Transform Infrared Spectroscopy (FTIR)

Fourier transform infrared spectroscopy was performed using a FTIR5700 Fourier infrared spectrum analyzer (Thermo Fisher, Waltham, MA, USA). The infrared spectra were measured over a wavelength range of 2000–1400 cm⁻¹.

2.6. Preparation of Coatings on Titanium

Commercially pure titanium discs (Ø8 mm × 0.7 mm) were purchased from Xijing Medical Equipment Co., Ltd. (Taiyuan, China). Ti discs were etched in 5 M NaOH at 60 °C for 12 h, washed with DI water and acetone, air dried, and immediately used for coatings (eTi). Three coating solutions were prepared by diluting the 10 mM GL13K stock solution to 1 mM in DI water, 90% ethanol solution, and 0.1 M carbonate–bicarbonate buffer (pH = 10), respectively. The etched Ti discs were incubated in the coating solutions overnight at room temperature (RT), rinsed with DI water, and dried under a stream of air.

2.7. Water Contact Angle (WCA) Measurement

WCA was measured using a contact angle goniometer (SL200KS) with CAST3.0 software (Kino Scientific Instrument Inc., Boston, MA, USA). A droplet of 1.0 µL DI water was deposited on a Ti disc and tracked for 20 s. WCA measurements were performed on two separate positions of four samples for each group (N = 8).

2.8. Bacterial Culture

Gram-positive *Staphylococcus aureus* (ATCC 25923) was used for the antimicrobial test in this study. *S. aureus* was inoculated in Trypticase Soy Broth (TSB; BD, Franklin Lakes, NJ, USA) and incubated in air at 37 °C and 100 rpm overnight. For enhancing antimicrobial activity, all samples were coated with D-GL13K (Gkiiklkaskll-NH₂, purity > 98%, Bankpeptide biological technology Co., Ltd., Hefei, China) [18]. Ti discs were UV-sterilized for 20 min on each side and then placed in the wells of a 48-well plate. Each sample was incubated in 1 mL TSB for 20 min first, then replaced with 1 mL diluted bacterial solution (OD₆₀₀ = 0.02). The samples were incubated in the bacterial solution in air at 37 °C and 100 rpm for 10 h.

2.9. ATP Assay

Viable bacteria on Ti discs after incubation were quantified using a BacTiter-Glo™ Microbial Cell Viability Assay (Promega, Madison, WI, USA). Samples were washed by 1 × PBS twice, transferred to a new 48-well plate, and washed one more time. The washed samples were incubated in a mixture of 200 µL BacTiter-Glo™ Reagent and 200 µL PBS in the dark at RT for 5 min. Afterwards, 200 µL of the mixture was transferred into a black 96-well plate to detect luminescence using a Tecan multimode microplate reader (Männedorf, Switzerland). An abiotic mixture was used as a control. Fifteen samples were tested for each group in two independent experiments (N = 15 per group). ATP luminescence was normalized to the average of the control group in the same experiment.

2.10. LIVE/DEAD Assay

Biofilms on Ti discs were stained using a LIVE/DEAD BBcellProbe™ N01/PI bacterial viability kit (BestBio Inc., Shanghai, China) in the dark at RT for 15 min and washed with a 0.9% sterile saline solution. Fluorescent microscopy was performed using a Leica confocal laser scanning microscope (CLSM; Wetzlar, Germany) at 10× magnification. Micrographs were taken in four different fields per group and processed with the Leica LAS X software.

2.11. Cytotoxicity Test

RAW 264.7 cells were used to evaluate the cytotoxicity of each group. Cells were cultured in Dulbecco's Modified Eagle Medium (DMEM) supplemented with 10% fetal bovine serum (FBS) at 37 °C in a 5% CO₂ humidified incubator. The medium was refreshed every third day. At passage 5, cells were passaged and seeded on the sample surfaces at a density of 10,000 cells/cm² and cultured for 1, 3 and 5 days. At each time point, a CCK-8 kit (Dojindo, Shanghai, China) was used to determine cellular metabolic activity, following the manufacturer's instructions. Briefly, the medium was replaced with fresh medium containing 10% CCK-8 reagent. After 2 h incubation, supernatant was transferred to a 96-well microplate and read at 450 nm with a microplate reader (Biotek, Winooski, VT, USA). The absorbance measured for each group was normalized against the noncoated control group.

2.12. Statistical Analysis

Statistical analysis was performed using IBM SPSS Statistics 25. Levene's test determined equal variances for the WCA, ATP assay, and CCK-8 assay results, so one-way ANOVA with Tukey HSD post hoc tests were performed.

3. Results and Discussion

3.1. Self-Assembly with α -Helices Formation in Ethanol Solutions

CD spectra revealed a mostly unordered (random coil) secondary structure for GL13K in water or a low-concentration (10%) ethanol solution with a negative band at 199 nm and very low ellipticity above 215 nm (Figure 1). In high-concentration (90% and 99%) ethanol solutions, GL13K presented a typical α -helix structure with negative bands at 222 nm and 208 nm and a positive band at 193 nm [27]. The $\theta_{222}/\theta_{208}$ ratios for GL13K in 90% and 99% ethanol solutions were around 0.6, indicating isolated α -helices without bundle formation [28]. When the ethanol and water volume fraction was 1:1 (50% ethanol), CD spectra showed a mixture of unordered and α -helix structures with a shifted negative band at 202 nm and the other unchanged negative band at around 222 nm. Estimations of secondary structures using CDPro confirmed the largely increased α -helix fractions (~70–75%) of GL13K in $\geq 50\%$ ethanol solutions (Table 1). We used TEM to further explore whether the formation of α -helix was caused by the reorganization of a single peptide molecule in the cosolvent or triggered by the self-assembly of the peptides into helical nanostructures, as a single peptide (MW = 1400 g/mol) cannot be visualized by TEM at the operating magnification.

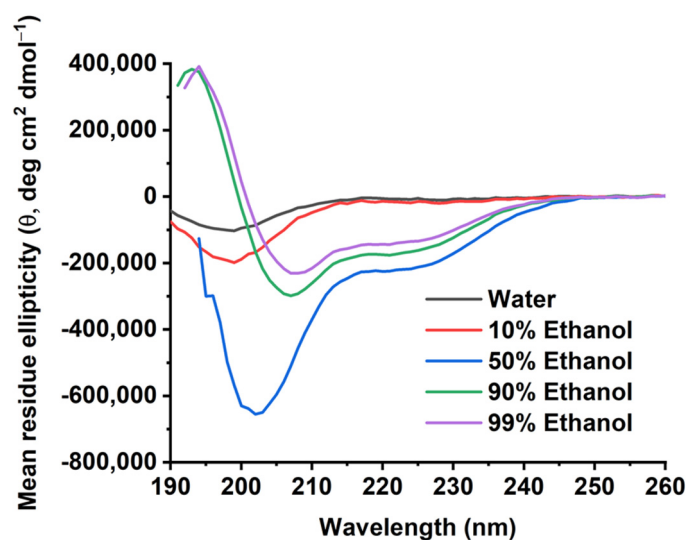
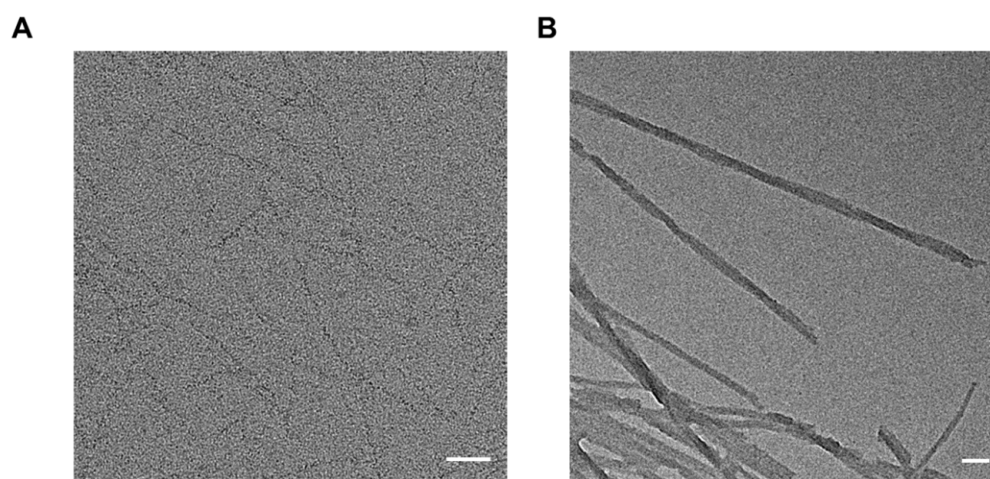


Figure 1. CD of 0.1 mM GL13K in water or ethanol solutions with ethanol volume fractions of 10%, 50%, 90%, and 99%.

Table 1. Fractions of secondary structures of GL13K in ethanol solutions estimated by CDPro.

Ethanol Volume Fraction (%)	α -Helix (%)	β -Sheet (%)	β -Turn (%)	Unordered (%)
10	1.3 \pm 0.7	9.9 \pm 5.3	6.6 \pm 3.2	81.8 \pm 9.1
50	75.5 \pm 12.1	5.8 \pm 8.8	5.0 \pm 4.8	16.0 \pm 5.3
90	75.1 \pm 4.6	0.9 \pm 3.0	7.5 \pm 1.5	19.0 \pm 12.9
99	70.3 \pm 6.9	5.1 \pm 4.6	7.6 \pm 2.4	17.5 \pm 10.5

In the 90% ethanol solution, thin nanofibers were observed with a diameter of \sim 3 nm and a length $>$ 100 nm (Figure 2A), demonstrating that the α -helix structure of GL13K was formed in a self-assembled state, but not as free peptides. In comparison, thick nanoribbons were present in a pH = 10 buffer solution with diameters of 10–40 nm that were consistent with previous studies [21,22]. Many AMPs are α -helical peptides, and their helicity was studied to be highly related to the antimicrobial activity and cytotoxicity against mammalian cells [29–31]. However, helical self-assembly of AMPs has been scarcely reported. E. Y. Lee et al. found that the association of three α -helical AMPs (LL37, melittin, and buforin) with DNA formed self-assembled protofibrils. The AMP–DNA complex presented immunomodulatory activity by amplifying Toll-like receptor 9 (TLR9) activation [32].

**Figure 2.** TEM images of self-assembled GL13K in (A) 90% ethanol solution and (B) pH = 10 buffer. Scale bars are 50 nm.

The different secondary structures and self-assembled morphologies in alkaline solutions or ethanol solutions were probably due to the different driven forces. In alkaline solutions, positive charges of Lys residues in GL13K are partially neutralized, resulting in a reduced electrostatic repulsion to trigger self-assembly [33]. For the α -helical self-assembly in the ethanol/water mixtures, hydrophobic interactions between peptide assemblies were enhanced by ethanol molecules [28]. Ethanol molecules can promote the hydrogen bonding among water molecules and remove water from the hydrophobic hydration shell of peptide assemblies. Similar self-assembled peptides with the formation of α -helices could be observed in 2,2,2-trifluoroethanol (TFE)/water cosolvent [34]. The exclusion of water molecules from the assembly hydration shell by TFE molecules was demonstrated using molecular dynamics simulation [35].

3.2. Ti Coatings with Free or Self-Assembled GL13K

We next investigate how the self-assembly and the formed secondary structures affect GL13K coatings. Alkaline-etched Ti surfaces (eTi) with activated hydroxyl groups were used as the model polar substrate. GL13K was prepared in water, 90% ethanol solution, and pH = 10 buffer to present as unordered free peptides, self-assembled peptides with the formation of α -helices, and self-assembled peptides with the formation of β -sheets, respectively. XPS

results showed characteristic N1s peaks from peptides (Figure 3A) and FTIR spectra revealed the presence of amide I and II peaks at 1660 cm^{-1} and 1558 cm^{-1} , respectively (Figure 3B), indicating the successful immobilization of GL13K on all three coatings. These results are consistent with the previously reported physisorbed GL13K on Ti [9,18].

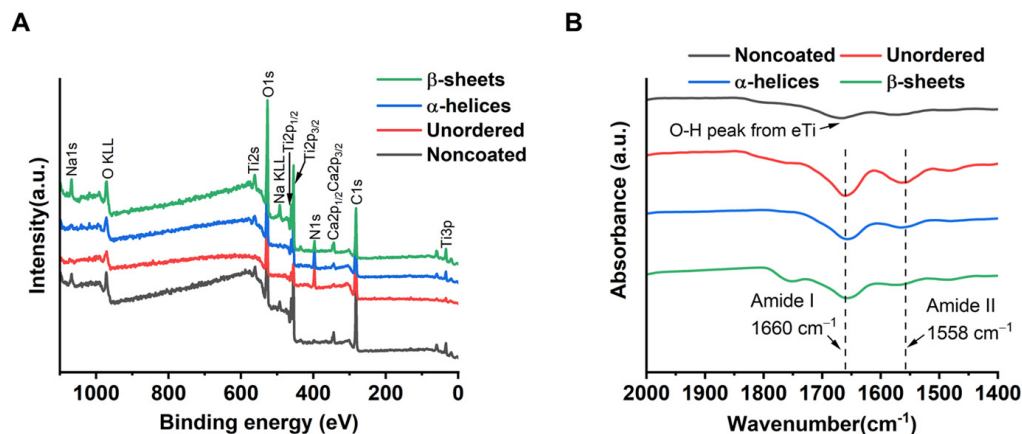


Figure 3. (A) XPS and (B) FTIR spectra of noncoated Ti or Ti coated with GL13K as unordered peptides, self-assembled α -helices, or self-assembled β -sheets.

As a result of the amphiphilicity of GL13K, all three coatings turned the highly hydrophilic Ti surface ($\text{WCA} < 15^\circ$) into hydrophobic surfaces (Figure 4). It is noted that there was a significant difference in the change in WCAs of the three coated surfaces, with WCA of $82.2 \pm 15.8^\circ$ for unordered GL13K, $132.5 \pm 7.2^\circ$ for self-assembled α -helices, and $107.1 \pm 19.5^\circ$ for self-assembled β -sheets, indicating a varied coating density and/or organization of hydrophobic and hydrophilic residues in GL13K coatings.

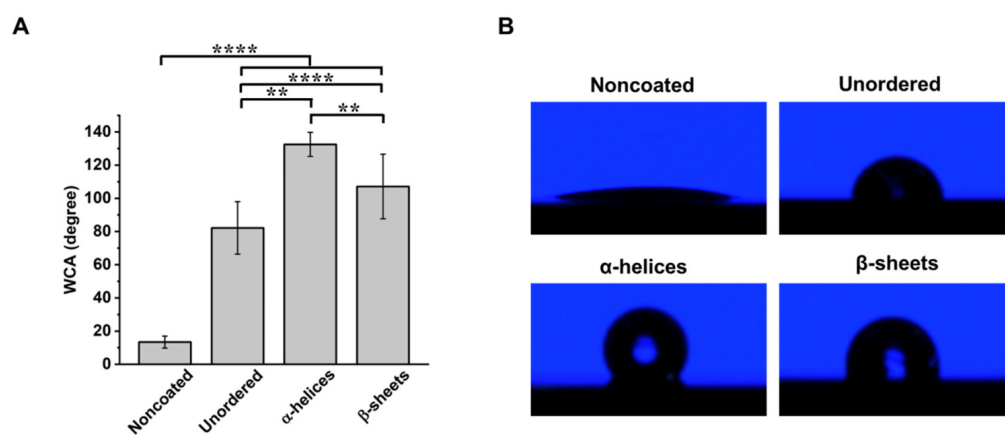


Figure 4. (A) WCA of noncoated Ti or Ti coated with GL13K as unordered peptides, self-assembled α -helices, or self-assembled β -sheets. $N = 8$ for each group. ** p -value < 0.01 , **** p -value < 0.0001 . (B) Representative images of sessile drops on different surfaces.

Both coatings with self-assembled GL13K, either in α -helix structure or β -sheet structure, had a significantly higher WCA than the coating with unordered free GL13K (Figure 4). The increased hydrophobicity was probably related to a higher coating density of GL13K as self-assemblies, leveraged by the strong hydrogen bonding between self-assembled GL13K and the polar substrate (i.e., etched Ti) [23]. When further comparing these two self-assembled GL13K coatings, the one with α -helices was more hydrophobic than the one with β -sheets (Figure 4), which might be due to a higher segregation of hydrophobic and hydrophilic residues in α -helices [36].

3.3. Antimicrobial Activity and Cytocompatibility of Different Coatings

The antimicrobial activity of the different GL13K coatings was tested against *S. aureus*, one of the most detected pathogens in implant infections [37]. Compared to the noncoated Ti control, all three GL13K coatings significantly reduced the viable bacteria on the surfaces (Figure 5A). Accordingly, bacteria with compromised membrane (stained red) were observed on the GL13K-coated surfaces compared to the noncoated surface with almost all live bacteria (stained green; Figure 5B). This indicated that physically coated GL13K maintained the antimicrobial activity irrespective of its self-assembling status or the secondary structures in the coatings.

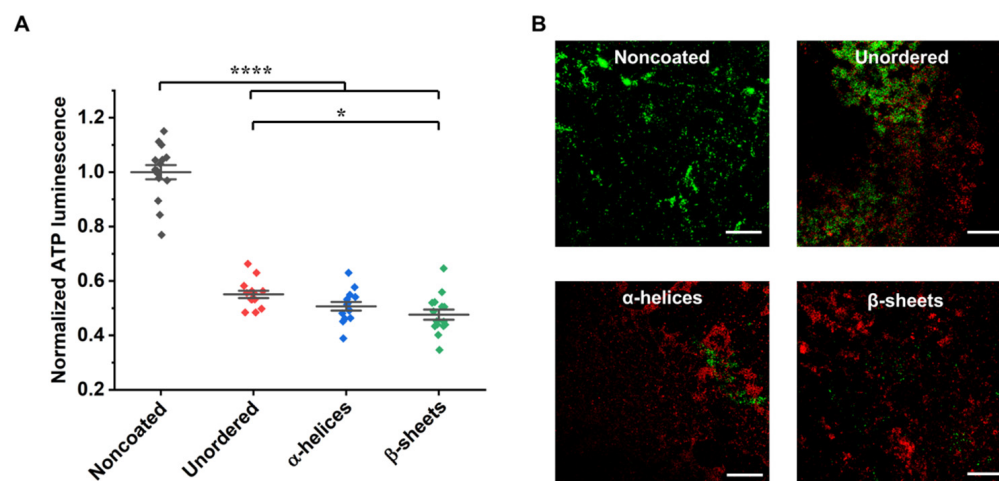


Figure 5. Antimicrobial test of the different coatings against *S. aureus*. (A) Normalized ATP luminescence intensity and (B) representative LIVE/DEAD CLSM images of colonized *S. aureus* on the Ti surfaces with no coatings or GL13K coatings prepared as unordered peptides, self-assembled α -helices, and self-assembled β -sheets. Scale bars are 50 μ m. N = 15 for each group. * p -value < 0.05, **** p -value < 0.0001.

The two self-assembled GL13K coatings (α -helices and β -sheets) had slightly less viable bacteria on the surfaces compared to the coating with unordered free GL13K (Figure 5). However, the difference was trivial, which might be due to the relatively short bacterial incubation period and/or testing against a single bacteria strain instead of multispecies. Furthermore, there was no obvious difference between the coatings with self-assembled α -helices and β -sheets, indicating that the secondary structure might not affect the antimicrobial activity of AMP coatings. We speculate that the increased antimicrobial activity of self-assembled GL13K might be related to a higher coating density, as we observed by QCM-D in our previous work [23]. The long-term coating stability and the in vivo antimicrobial activity need to be further assessed in future work [18]. All physisorbed GL13K coatings were cytocompatible with RAW 264.7 cells, with no significant differences in proliferation after 1, 3, and 5 days (Figure 6).

The new strategy of preparing self-assembled AMPs in ethanol solutions to form stable antimicrobial coatings envisions a simple and safe in situ coating method. Many applications require direct coatings on sites, such as implant-retention surgeries [38,39] or priming dentin in resin composite restorations [19,40], which would not be feasible by the intense covalent immobilization methods. Furthermore, the significantly enhanced hydrophobicity leveraged from the self-assembled α -helices might promote the coating resistance to waterborne degradation of peptides by proteases.

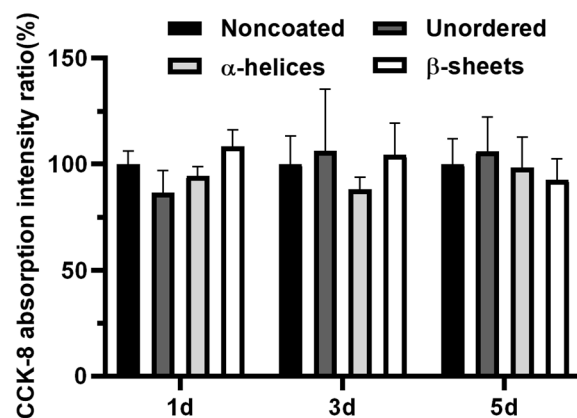


Figure 6. Cell proliferation of RAW 264.7 cells assessed by CCK-8 cell viability assay. No statistical difference was found among the tested groups (p -value < 0.05). $N = 4$ for each group at each time point.

4. Conclusions

We triggered AMP self-assembly with the formation of α -helices in ethanol/water cosolvent which presented a different morphology from the β -sheet-formed self-assembly in alkaline solutions. Physical AMP coatings were formed on alkaline-etched Ti by GL13K in three different conditions: unordered free peptides, self-assembled α -helices, and self-assembled β -sheets. The XPS and FTIR results confirmed the successful coatings of all three physisorbed GL13K conditions. Compared to the unordered free GL13K, self-assemblies with either α -helices or β -sheets enhanced the coating hydrophobicity and antimicrobial activity, which might be due to a higher coating density.

Author Contributions: Conceptualization, Z.Y.; methodology, X.Z., W.T., X.C., H.W., T.S. and Z.Y.; formal analysis, X.Z., T.S. and Z.Y.; investigation, X.Z., T.S. and Z.Y.; funding acquisition, X.Z. and T.S.; resources, X.Z., T.S. and Z.Y.; data curation, X.Z., T.S. and Z.Y.; writing—original draft preparation, Z.Y.; writing—review and editing, X.Z., T.S. and Z.Y. All authors have read and agreed to the published version of the manuscript.

Funding: This research was supported by the National Natural Science Foundation of China (Grant No. 82160190 to T.S.), the Jiangxi Provincial Department of Science and Technology, China (Grant No. 20203BBGL73156 to T.S., 20192BBG70022 to T.S.), and the Hubei Provincial Department of Science and Technology, China (Grant No. 2020CFB252 to X.Z.).

Institutional Review Board Statement: Not applicable.

Informed Consent Statement: Not applicable.

Data Availability Statement: Not applicable.

Conflicts of Interest: The authors declare no conflict of interest.

References

1. Arciola, C.R.; Campoccia, D.; Montanaro, L. Implant Infections: Adhesion, Biofilm Formation and Immune Evasion. *Nat. Rev. Microbiol.* **2018**, *16*, 397–409. [[CrossRef](#)] [[PubMed](#)]
2. Busscher, H.J.; Rinastiti, M.; Siswomihardjo, W.; Van Der Mei, H.C. Biofilm Formation on Dental Restorative and Implant Materials. *J. Dent. Res.* **2010**, *89*, 657–665. [[CrossRef](#)] [[PubMed](#)]
3. Li, B.; Webster, T.J. Bacteria Antibiotic Resistance: New Challenges and Opportunities for Implant-Associated Orthopedic Infections. *J. Orthop. Res.* **2018**, *36*, 22–32. [[CrossRef](#)]
4. Wei, H.; Song, X.; Liu, P.; Liu, X.; Yan, X.; Yu, L. Antimicrobial Coating Strategy to Prevent Orthopaedic Device-Related Infections: Recent Advances and Future Perspectives. *Biomater. Adv.* **2022**, *135*, 212739. [[CrossRef](#)] [[PubMed](#)]
5. Riool, M.; De Breij, A.; Drijfhout, J.W.; Nibbering, P.H.; Zaat, S.A.J. Antimicrobial Peptides in Biomedical Device Manufacturing. *Front. Chem.* **2017**, *5*, 63. [[CrossRef](#)] [[PubMed](#)]
6. Kazemzadeh-Narbat, M.; Cheng, H.; Chabok, R.; Alvarez, M.M.; De La Fuente-Nunez, C.; Phillips, K.S.; Khademhosseini, A. Strategies for Antimicrobial Peptide Coatings on Medical Devices: A Review and Regulatory Science Perspective. *Crit. Rev. Biotechnol.* **2021**, *41*, 94–120. [[CrossRef](#)]

7. Chen, R.; Willcox, M.D.; Ho, K.K.K.; Smyth, D.; Kumar, N. Antimicrobial Peptide Melimine Coating for Titanium and Its In Vivo Antibacterial Activity in Rodent Subcutaneous Infection Models. *Biomaterials* **2016**, *85*, 142–151. [[CrossRef](#)]
8. Kazemzadeh-Narbat, M.; Lai, B.F.; Ding, C.; Kizhakkedathu, J.N.; Hancock, R.; Wang, R. Multilayered Coating on Titanium for Controlled Release of Antimicrobial Peptides for the Prevention of Implant-Associated Infections. *Biomaterials* **2013**, *34*, 5969–5977. [[CrossRef](#)]
9. Holmberg, K.V.; Abdolhosseini, M.; Li, Y.; Chen, X.; Gorr, S.-U.; Aparicio, C. Bio-Inspired Stable Antimicrobial Peptide Coatings for Dental Applications. *Acta Biomater.* **2013**, *9*, 8224–8231. [[CrossRef](#)]
10. Mishra, B.; Basu, A.; Chua, R.R.Y.; Saravanan, R.; Tambyah, P.A.; Ho, B.; Chang, M.W.; Leong, S.S.J. Site Specific Immobilization of a Potent Antimicrobial Peptide onto Silicone Catheters: Evaluation against Urinary Tract Infection Pathogens. *J. Mater. Chem. B* **2014**, *2*, 1706–1716. [[CrossRef](#)]
11. Singha, P.; Locklin, J.; Handa, H. A Review of the Recent Advances in Antimicrobial Coatings for Urinary Catheters. *Acta Biomater.* **2017**, *50*, 20–40. [[CrossRef](#)] [[PubMed](#)]
12. Willcox, M.; Hume, E.; Aliwarga, Y.; Kumar, N.; Cole, N. A Novel Cationic-Peptide Coating for the Prevention of Microbial Colonization on Contact Lenses. *J. Appl. Microbiol.* **2008**, *105*, 1817–1825. [[CrossRef](#)] [[PubMed](#)]
13. Dutta, D.; Vijay, A.K.; Kumar, N.; Willcox, M. Melimine-Coated Antimicrobial Contact Lenses Reduce Microbial Keratitis in an Animal Model. *Investig. Ophthalmology Vis. Sci.* **2016**, *57*, 5616–5624. [[CrossRef](#)] [[PubMed](#)]
14. Costa, F.; Carvalho, I.F.; Montelaro, R.C.; Gomes, P.; Martins, M.C.L. Covalent Immobilization of Antimicrobial Peptides (AMPs) onto Biomaterial Surfaces. *Acta Biomater.* **2011**, *7*, 1431–1440. [[CrossRef](#)] [[PubMed](#)]
15. Shukla, A.; Fleming, K.E.; Chuang, H.F.; Chau, T.M.; Loose, C.R.; Stephanopoulos, G.N.; Hammond, P.T. Controlling the Release of Peptide Antimicrobial Agents from Surfaces. *Biomaterials* **2010**, *31*, 2348–2357. [[CrossRef](#)] [[PubMed](#)]
16. Kazemzadeh-Narbat, M.; Kindrachuk, J.; Duan, K.; Jenssen, H.; Hancock, R.E.; Wang, R. Antimicrobial Peptides on Calcium Phosphate-Coated Titanium for the Prevention of Implant-Associated Infections. *Biomaterials* **2010**, *31*, 9519–9526. [[CrossRef](#)] [[PubMed](#)]
17. Ma, M.; Kazemzadeh-Narbat, M.; Hui, Y.; Lu, S.; Ding, C.; Chen, D.D.Y.; Hancock, R.E.W.; Wang, R. Local Delivery of Antimicrobial Peptides Using Self-Organized TiO₂ Nanotube arrays for Peri-Implant Infections. *J. Biomed. Mater. Res. Part A* **2012**, *100A*, 278–285. [[CrossRef](#)]
18. Ye, Z.; Sang, T.; Li, K.; Fischer, N.G.; Mutreja, I.; Echeverría, C.; Kumar, D.; Tang, Z.; Aparicio, C. Hybrid Nanocoatings of Self-Assembled Organic-Inorganic Amphiphiles for Prevention of Implant Infections. *Acta Biomater.* **2022**, *140*, 338–349. [[CrossRef](#)]
19. Moussa, D.; Kirihara, J.; Ye, Z.; Fischer, N.; Khot, J.; Witthuhn, B.; Aparicio, C. Dentin Priming with Amphiphilic Antimicrobial Peptides. *J. Dent. Res.* **2019**, *98*, 1112–1121. [[CrossRef](#)]
20. Ye, Z.; Zhu, X.; Mutreja, I.; Boda, S.K.; Fischer, N.G.; Zhang, A.; Lui, C.; Qi, Y.; Aparicio, C. Biomimetic Mineralized Hybrid Scaffolds with Antimicrobial Peptides. *Bioact. Mater.* **2021**, *6*, 2250–2260. [[CrossRef](#)]
21. Ye, Z.; Zhu, X.; Acosta, S.; Kumar, D.; Sang, T.; Aparicio, C. Self-Assembly Dynamics and Antimicrobial Activity of All L- and d-Amino acid Enantiomers of a Designer Peptide. *Nanoscale* **2019**, *11*, 266–275. [[CrossRef](#)] [[PubMed](#)]
22. Ye, Z.; Aparicio, C. Modulation of Supramolecular Self-Assembly of an Antimicrobial Designer Peptide by Single Amino Acid Substitution: Implications on Peptide Activity. *Nanoscale Adv.* **2019**, *1*, 4679–4682. [[CrossRef](#)] [[PubMed](#)]
23. Ye, Z.; Kobe, A.C.; Sang, T.; Aparicio, C. Unraveling Dominant Surface Physicochemistry to Build Antimicrobial Peptide Coatings with Supramolecular Amphiphiles. *Nanoscale* **2020**, *12*, 20767–20775. [[CrossRef](#)] [[PubMed](#)]
24. Wang, M.; Wang, J.; Zhou, P.; Deng, J.; Zhao, Y.; Sun, Y.; Yang, W.; Wang, D.; Li, Z.; Hu, X.; et al. Nanoribbons Self-Assembled from Short Peptides Demonstrate the Formation of Polar Zippers between β -Sheets. *Nat. Commun.* **2018**, *9*, 5118. [[CrossRef](#)]
25. Ahmed, T.; Hammami, R. Recent insights into structure-function relationships of antimicrobial peptides. *J. Food Biochem.* **2019**, *43*, e12546. [[CrossRef](#)]
26. Ye, Z.; Aparicio, C. Interactions of Two Enantiomers of a Designer Antimicrobial Peptide with Structural Components of the Bacterial Cell Envelope. *J. Pept. Sci.* **2022**, *28*, e3299. [[CrossRef](#)]
27. Greenfield, N.J. Using Circular Dichroism Spectra to Estimate Protein Secondary Structure. *Nat. Protoc.* **2007**, *1*, 2876–2890. [[CrossRef](#)]
28. Nandakumar, A.; Ito, Y.; Ueda, M. Solvent Effects on the Self-Assembly of an Amphiphilic Polypeptide Incorporating α -Helical Hydrophobic Blocks. *J. Am. Chem. Soc.* **2020**, *142*, 20994–21003. [[CrossRef](#)]
29. Xiong, M.; Lee, M.W.; Mansbach, R.A.; Song, Z.; Bao, Y.; Peek, R.M.; Yao, C.; Chen, L.-F.; Ferguson, A.L.; Wong, G.C.L.; et al. Helical Antimicrobial Polypeptides with Radial Amphiphilicity. *Proc. Natl. Acad. Sci. USA* **2015**, *112*, 13155–13160. [[CrossRef](#)]
30. Zelezetsky, I.; Tossi, A. Alpha-helical antimicrobial peptides—Using a sequence template to guide structure–activity relationship studies. *Biochim. Biophys. Acta (BBA)-Biomembr.* **2006**, *1758*, 1436–1449. [[CrossRef](#)]
31. Huang, Y.; He, L.; Li, G.; Zhai, N.; Jiang, H.; Chen, Y. Role of helicity of α -helical antimicrobial peptides to improve specificity. *Protein Cell* **2014**, *5*, 631–642. [[CrossRef](#)]
32. Lee, E.Y.; Zhang, C.; Di Domizio, J.; Jin, F.; Connell, W.; Hung, M.; Malkoff, N.; Veksler, V.; Gilliet, M.; Ren, P.; et al. Helical antimicrobial peptides assemble into protofibril scaffolds that present ordered dsDNA to TLR9. *Nat. Commun.* **2019**, *10*, 1012. [[CrossRef](#)] [[PubMed](#)]
33. Mandal, D.; Nasrolahi Shirazi, A.; Parang, K. Self-Assembly of Peptides to Nanostructures. *Org. Biomol. Chem.* **2014**, *12*, 3544–3561. [[CrossRef](#)] [[PubMed](#)]

34. Han, S.-H.; Lee, M.-K.; Lim, Y.-B. Bioinspired Self-Assembled Peptide Nanofibers with Thermostable Multivalent α -Helices. *Biomacromolecules* **2013**, *14*, 1594–1599. [[CrossRef](#)] [[PubMed](#)]
35. Roccatano, D.; Colombo, G.; Fioroni, M.; Mark, A.E. Mechanism by Which 2,2,2-Trifluoroethanol/Water Mixtures Stabilize Secondary-Structure Formation in Peptides: A molecular dynamics study. *Proc. Natl. Acad. Sci. USA* **2002**, *99*, 12179–12184. [[CrossRef](#)] [[PubMed](#)]
36. Khara, J.S.; Obuobi, S.; Wang, Y.; Hamilton, M.S.; Robertson, B.D.; Newton, S.M.; Yang, Y.Y.; Langford, P.R.; Ee, P.L.R. Disruption of Drug-Resistant Biofilms Using de novo Designed Short α -Helical Antimicrobial Peptides with Idealized Facial Amphiphilicity. *Acta Biomater.* **2017**, *57*, 103–114. [[CrossRef](#)]
37. Oliveira, W.; Silva, P.; Silva, R.; Silva, G.; Machado, G.; Coelho, L.; Correia, M. Staphylococcus aureus and Staphylococcus epidermidis infections on implants. *J. Hosp. Infect.* **2018**, *98*, 111–117. [[CrossRef](#)]
38. Tran, H.A.; Tran, P.A. In Situ Coatings of Silver Nanoparticles for Biofilm Treatment in Implant-Retention Surgeries: Antimicrobial Activities in Monoculture and Coculture. *ACS Appl. Mater. Interfaces* **2021**, *13*, 41435–41444. [[CrossRef](#)]
39. A Tran, H.; A Tran, P. Immobilization-Enhanced Eradication of Bacterial Biofilms and in situ Antimicrobial Coating of Implant Material Surface—An in vitro Study. *Int. J. Nanomed.* **2019**, *ume 14*, 9351–9360. [[CrossRef](#)]
40. Moussa, D.G.; Fok, A.; Aparicio, C. Hydrophobic and antimicrobial dentin: A peptide-based 2-tier protective system for dental resin composite restorations. *Acta Biomater.* **2019**, *88*, 251–265. [[CrossRef](#)]